

CATCHING THE BIRTH OF A DARK MOLECULAR CLOUD FOR THE FIRST TIME

PEI ZUO^{1,2}

National Astronomical Observatories, Chinese Academy of Sciences, Datun Road, Chaoyang District, Beijing 100101, China and
University of Chinese Academy of Sciences, Beijing 100049, China

DI LI^{1,2,3}

National Astronomical Observatories, Chinese Academy of Sciences, Datun Road, Chaoyang District, Beijing 100101, China
University of Chinese Academy of Sciences, Beijing 100049, China and
Key Laboratory of Radio Astronomy, Chinese Academy of Sciences, Nanjing, 210008, China

J. E. G. PEEK⁴

Space Telescope Science Institute, 3700 San Martin Drive, Baltimore, MD 21218, USA

QIANG CHANG⁵

Xinjiang Astronomical Observatory, Chinese Academy of Sciences, 150 Science 1-Street, Urumqi, Xinjiang 830011, China

XIA ZHANG⁵

Xinjiang Astronomical Observatory, Chinese Academy of Sciences, 150 Science 1-Street, Urumqi, Xinjiang 830011, China

NICHOLAS CHAPMAN⁶

CIERA - Northwestern University 2145 Sheridan Road Evanston, IL 60208, USA

PAUL F. GOLDSMITH⁷

Jet Propulsion Laboratory, California Institute of Technology, Pasadena, CA 91109, USA

AND

ZHI-YU ZHANG^{8,9}

Institute for Astronomy, University of Edinburgh, Royal Observatory, Blackford Hill, Edinburgh EH9 3HJ, UK and
ESO, Karl Schwarzschild Strasse 2, D-85748 Garching, Munich, Germany

Draft version October 26, 2018

ABSTRACT

The majority of hydrogen in the interstellar medium (ISM) is in atomic form. The transition from atoms to molecules and, in particular, the formation of the H₂ molecule, is a key step in cosmic structure formation en route to stars. Quantifying H₂ formation in space is difficult, due to the confusion in the emission of atomic hydrogen (HI) and the lack of a H₂ signal from the cold ISM. Here we present the discovery of a rare, isolated dark cloud currently undergoing H₂ formation, as evidenced by a prominent “ring” of HI self-absorption. Through a combined analysis of HI narrow self-absorption, CO emission, dust emission, and extinction, we directly measured, for the first time, the [HI]/[H₂] abundance varying from 2% to 0.2%, within one region. These measured HI abundances are orders of magnitude higher than usually assumed initial conditions for protoplanetary disk models. None of the fast cloud formation model could produce such low atomic hydrogen abundance. We derived a cloud formation time scale of 6×10^6 years, consistent with the global Galactic star formation rate, and favoring the classical star formation picture over fast star formation models. Our measurements also help constrain the H₂ formation rate, under various ISM conditions.

Keywords: ISM: star formation — ISM: molecular cloud — ISM: atomic hydrogen

1. INTRODUCTION

The formation of the H₂ molecules is a key process in converting atoms into molecules in the interstellar medium (ISM) and is the critical step in the formation of stars. Spitzer (1946) suggested that H₂ formation occurs on dust grains, rather than in the gas phase,

because the collision frequency is too low to provide sufficient three-body collisions in molecular clouds (Kaiser 2002). A widely accepted description of an efficient HI–H₂ transformation process in clouds is provided by Hollenbach & Salpeter (1971). Efficient H₂ formation can persist to high temperatures because chemisorbed atoms can stay on the grain surface while maintaining quantum mobility. Such configuration is conducive to hydrogen recombination (H₂ formation) until the dust grain surface temperature reaches ~ 500 K (Cazaux &

peizuo@nao.cas.cn

¹ National Astronomical Observatories, Chinese Academy of Sciences, Datun Road, Chaoyang District, Beijing 100012, China

Tielens 2004). Laboratory experiments demonstrated that H_2 formation could also occur on carbon surfaces with a high recombination efficiency over a broad range of temperature (Vidali et al. 2005). The theoretical work in Cazaux et al. (2005) explained the high efficiency under low temperatures in both quiescent diffuse and dense clouds in terms of physisorption forces and thermally activated diffusion. Since the timescale of star formation is tightly constrained by the timescale of molecular gas formation, it is crucial to have a self-consistent understanding of the global star formation efficiency and star formation rate in galaxies. The timescale of star formation is controversial. The canonical model (Shu 1977) favored it to be around 10 Myr, while Bergin et al. (2004) and Elmegreen (2000), hypothesized that star formation occurs on a turbulent crossing scale that corresponds to about only 1 Myr on parsec scales (Glover & Mac Low 2007).

Direct measurement of H_2 formation is difficult because HI is hard to isolate in the Galaxy and H_2 lacks a permanent dipole moment, making it rare to have both measurements of HI and H_2 gas for the same regions of the Galaxy. Key physical parameters need largely to be assumed in calculating cloud formation. Molecular hydrogen can be observed through absorption if it is against a good X-ray and/or ultraviolet background source (e.g. Sembach et al. (2001)). Since H_2 itself does not emit at the temperature of molecular clouds, these regions are generally traced emission from the lower rotational transitions of CO. However, subthermal excitation in diffuse gas and depletion in dense gas make CO unsatisfactory to trace H_2 (Kramer et al. 1999). It is also difficult to probe the cloud formation timescale through astrochemistry based on molecular species other than H_2 and HI, such as N_2H^+ and deuterated species (Caselli et al. 2002), because these tracers comprise only a tiny fraction of cloud mass. The foremost chemical reaction in molecular formation is the formation of molecular hydrogen. It is thus paramount for us to obtain direct measurement of the H_2 formation timescale in order to better understand cloud formation timescale, the star formation efficiency and the star formation rate.

We have developed an observational method called HI Narrow Self-Absorption (HiNSA; (Li & Goldsmith 2003; Goldsmith & Li 2005)), which is capable of measuring atomic hydrogen abundance in dense clouds. Similar to the well-known HI Self-Absorption (HiSA (Heeschen 1955)) phenomenon in the cold neutral medium (CNM), HiNSA differs in a significant aspect, namely, the thermalization of HI at low temperatures through collisions with H_2 . Due to efficient cooling by molecular emission lines, especially the rotational transitions of CO, molecular clouds claim most of the lowest temperatures found in the Milky Way except for a few rare cases, such as those discussed by Knee & Brunt (2001) and Peek et al. (2011b). In contrast, lacking molecular cooling, HiSA is likely a result of temperature fluctuations in the CNM (Gibson et al. 2000). Systematic surveys have shown that HiNSA is associated with molecular clouds (Krčo & Goldsmith 2010), and thus provides a direct measurement of cold HI in dark clouds.

The left image in Figure 2 gives a schematic diagram of the transition from CNM to dense molecular gas. In the warm ionized medium (WIM) and HII regions,

hydrogen is largely in the form of H^+ . For higher densities and lower UV intensities, H^+ combines with electrons through radiative recombination and forms HI. With increasing HI volume density, hydrogen atoms start to form molecular hydrogen on the surface of dust grains. In diffuse molecular clouds, even when most of the H is in the molecular form, gas-phase carbon can still be mainly C^+ . After combining with H_2 through radiative association, C^+ becomes CH_2^+ ; CH_2^+ reacts rapidly with electrons to form CH; then CH reacts with O to produce CO. C^+ can also react with electrons to form CI through dielectronic recombination. CI, along with OH, lead the formation of CO through neutral-neutral reactions in colder ($10\text{ K} < T < 100\text{ K}$) dark clouds (Woodall et al. 2007). Other molecules form following CO in dense cores. In particular, N_2H^+ , NH_3 , and cations like H_2D^+ become significant and have been used to study the cloud core formation time scale (Brünken et al. 2014).

Isolated, cold dark clouds are the ideal laboratory for studying H_2 formation in the Milky Way. In a previous study, B227, CB45, and L1574, were identified as isolated dark clouds, and coincidentally aligned in a linear configuration from north to south spanning about two degrees (Martin & Barrett 1978). There are no nearby UV sources such as massive stars or HII regions.

In this paper, we present a combined analysis of HiNSA, CO emission, dust emission, and extinction for a rare, isolated dark cloud, currently undergoing H_2 formation. The $[\text{HI}]/[\text{H}_2]$ abundance varies from 2% to 0.2%, within one region and the formation timescale was derived as ~ 6 Myrs, which is consistent with both an analytical model and a numerical chemistry model.

2. OBSERVATIONS AND DATA REDUCTION

To reconstruct the chemical state and the evolutionary history of isolated dark clouds, we mapped HI, $^{13}\text{CO } J = 1 - 0$ emission, and dust continuum emission in B227, CB45, and L1574, which were identified as HiNSA sources by Goldsmith & Li (2005). In 2012 May and November, the sources were observed in the 1420 MHz transition of HI using the Arecibo *L*-band Feed Array (ALFA) on the 305 m radio telescope. We implemented the observations in the “total power” mode because of a clear “off” position that was difficult to find in the Galaxy. The nominal system temperature of 30 K has contributions from the system temperature and the HI emission. In addition, the temperature of the HI emission from standard CNM is around 70 K (Heiles & Troland 2003). Hence, we consider an equivalent system temperature of 100 K for evaluating the observing sensitivity. To accomplish the mapping for the sources that extend $1^\circ \times 2^\circ$, the “leap frog” drift scan was adopted (Minchin et al. 2007). Spectra were recorded by GALSPECT, the Galactic ALFA spectrometer. The resolution is 0.18 km s^{-1} per channel with 7,679 channels. Using the Spectral and Photometric Imaging Receiver (SPIRE) on board the *Herschel Space Observatory*, the sources (B227, L1574, and CB45) were observed at 250, 350, and $500\ \mu\text{m}$ on 2011 September 11 within a *Herschel* Open Time (OT) 1 Program (OT1_dli_2). In the fast mapping mode having a nominal scan speed of $30''\text{ s}^{-1}$, two $9'$ legs were used at each band for mapping each of the sources covered by the scanned area of $30' \times 30'$. ^{13}CO

data were taken with the Five College Radio Astronomy Observatory (FCRAO) and adapted from [Goldsmith & Li \(2005\)](#).

Our SPIRE data were processed by using the software package HIPE². The original image at each band was produced based on a zero-median brightness. To calibrate the offsets between bands, the ZEROPOINT-CORRECTION subroutine was used, which implements a cross-calibration with the *Planck* HFI-545 and HFI-857 images and a color correction HFI to SPIRE wavebands assuming a gray body function with fixed beta. We used the subroutine BASELINE REMOVAL AND DESTRIPE to remove the baseline with correcting the relative gain of the bolometer. PHOTOMETER MAP MERGING was then used to merge the images of the bands. The Arecibo HI data were processed following the procedure of the GALFA-HI Standard Reduction ([Peek et al. 2011a](#)). It is designed for the ALFA in order to take the time-ordered data (TOD) that come out of GALSPECT, over a single region and turn it into a calibrated, gridded spectral (PPV) data cube. The resulting data also showed stripes along the scan direction, we destriped the data by running the procedure to use the places of the data cross each other to self-calibrate the gains of each beam. We obtained Two Micron All Sky Survey (2MASS) extinction data based on the *J*, *H*, and *K_s* bands of the 2MASS data. ¹³CO data were taken with FCRAO and adapted from [Goldsmith & Li \(2005\)](#). We regrided the pixel onto a 1' grid in order to match the HI data.

3. DUST, COLD HI AND ¹³CO

Our new continuous, Nyquist-sampled HI map complemented by ¹³CO and dust images enables us to identify a striking HiNSA ring and directly measure the variation of HI abundance in these transition clouds (Figure 1).

3.1. Dust Temperature and Column Density

For each image pixel, an SED was extracted and fitted with a single-temperature modified blackbody of the form

$$S_\nu = \Omega B_\nu(\nu, T_d) \kappa_\nu \mu m_H N_{H_2}, \quad (1)$$

where Ω is the solid angle of the emitting element, B_ν is the blackbody emission from the dust at temperature T_d , κ_ν is the dust mass absorption coefficient, $\mu = 2.33$ is the particle mass per hydrogen molecule, m_H is the mass of hydrogen atom, and N_{H_2} is the column density of hydrogen molecules, and we assumed the gas-to-dust ratio is 100. In Equation (1),

$$B_\nu(\nu, T_d) = \frac{2h\nu^3}{c^2} \frac{1}{e^{(h\nu/kT_d)} - 1} \quad (2)$$

is the Planck function and

$$\kappa_\nu = \kappa_{230} \left(\frac{\nu}{230 \text{ GHz}} \right)^\beta, \quad (3)$$

(where $\kappa_{230} = 0.009 \text{ cm}^2 \text{ g}^{-1}$) is the emissivity of the dust grains at 230 GHz.

We used 2MASS extinction data to eliminate the column density of hydrogen atoms as a parameter for

fitting the dust temperature T_d and emissivity spectral index β . The hydrogen column density N_H can be estimated from the optical extinction ([Güver & Özel 2009](#)),

$$\frac{N_H}{\text{cm}^{-2}} = 2.2 \times 10^{21} \left(\frac{A_v}{\text{mag}} \right). \quad (4)$$

As the atomic hydrogen fractional abundance is small, we take $N_{H_I} = 0$ and obtain

$$N_H = 2N_{H_2}. \quad (5)$$

The column density of hydrogen molecules N_{H_2} is related to visual extinction A_v ,

$$\frac{N_{H_2}}{\text{cm}^{-2}} = 1.1 \times 10^{21} \left(\frac{A_v}{\text{mag}} \right). \quad (6)$$

Combined *Herschel* SPIRE 250, 350 and 500 μm data with 2MASS extinction data, the dust temperature T_d , column density of hydrogen molecules N_{H_2} and emissivity spectral index β can be fitted simultaneously by using Equation (1).

3.2. Column Density of Cold HI

The new Arecibo HI images provide us with the overall HiNSA distribution in these sources. In order to extract the absorption component, we subtracted a relatively uniform background by averaging the HI emission values from surrounding points of the clouds, which has been done in a fashion similar to that described by [Knee & Brunt \(2001\)](#). The method for solving for the optical depth of the absorbing gas is described from Eq. 12 in [Li & Goldsmith \(2003\)](#),

$$\tau_0 = \ln \left[\frac{pT_{H_I} + (T_c - T_x)(1 - \tau_f)}{pT_{H_I} + (T_c - T_x)(1 - \tau_f) - T_{ab}} \right], \quad (7)$$

where τ_0 is the peak optical depth of the absorption feature at the centroid velocity, τ_f is the foreground HI optical depth, taken to be 0.1, which is the typical value of the foreground HI and only results in 0.4% uncertainty of optical depth of HI. T_{H_I} is the quantity obtained from the spectrum by fitting a polynomial to the portion of the spectrum without the absorption, T_c is continuum temperature, taken to be 3.5 K, including the cosmic background and Galactic continuum emission. T_x is the excitation temperature of HI in the dark cloud, which could be replaced by the dust temperature, T_{ab} is the absorption temperature, which is referred to as the depth of absorption line, p is the ratio of background HI optical depth τ_b to optical depth of the uniformed Galactic atomic gas τ_h ($\tau_b = p\tau_h$), τ_h is the total of the foreground HI optical depth and the background HI optical depth ($\tau_h = \tau_f + \tau_b$), and p can be calculated from a model of the local HI distribution and is generally in the range of 0.8-0.9.

The column density of HI is given by

$$\frac{N_{\text{HiNSA}}}{\text{cm}^{-2}} = 1.95 \times 10^{18} \tau_0 \frac{\Delta V}{\text{km s}^{-1}} \frac{T_k}{\text{K}}, \quad (8)$$

where ΔV is the FWHM of the absorption line from a Gaussian fit, and T_k is the kinetic temperature. We used the dust temperature T_d derived from *Herschel* SPIRE

² <http://http://herschel.esac.esa.int/hipe/>; version 13.0.0

maps as T_k , which should be well coupled in such clouds (Goldsmith & Li 2005). The column density of cold HI had been obtained based on HiNSA analysis.

Since the true total column density measurement will be affected by the optically thin approximation, several approaches have been employed to evaluate this potential problem. Lee et al. (2015) used two different methods to estimate the correction factor f for high optical depth and found that they are consistent, which is likely due to the relatively low optical depth and insignificant contribution from the diffuse radio continuum emission. As the clouds we study are located in the outer region of the Galaxy and the optical depths are small (Kolpak et al. 2002), the correction for the optical depth should not affect the HI column density significantly. The overall uncertainty is approximately 50%.

Since we cannot obtain the T_k , we present the upper and lower limit HI column density and HI abundance by using temperature of 10 and 30 K. The upper and lower limits for the HI column density for the three clouds are $7.50 \times 10^{19} \text{cm}^{-2}$ and $2.31 \times 10^{18} \text{cm}^{-2}$ respectively. The upper and lower limits for the HI abundance are 0.09 and 0.001 respectively.

3.3. ^{13}CO Column Density

The central frequency of the ^{13}CO $J = 1 - 0$ line ν is 110.2 GHz.

The column density of ^{13}CO in the upper level ($J = 1$) can be expressed as

$$N_{\text{u},^{13}\text{CO}} = \frac{8\pi k\nu^2}{hc^3 A_{\text{ul}}} \int T_{\text{b}} dv, \quad (9)$$

where k is Boltzmann's constant, h is Planck's constant, c is the speed of light, A_{ul} is the spontaneous decay rate from the upper level to the lower level, and T_{b} is the brightness temperature. We obtain

$$\left(\frac{N_{\text{u},^{13}\text{CO}}}{\text{cm}^{-2}} \right) = 3.7 \times 10^{14} \int \left(\frac{T_{\text{b}}}{\text{K}} \right) d \left(\frac{v}{\text{km s}^{-1}} \right). \quad (10)$$

The total ^{13}CO column density N_{tot} is related to the upper level column density N_{u} through

$$N_{\text{tot},^{13}\text{CO}} = f_{\text{u}} f_{\tau} f_{\text{b}} N_{\text{u},^{13}\text{CO}}, \quad (11)$$

where the level correction factor f_{u} can be calculated analytically under the assumption of local thermal equilibrium (LTE) as

$$f_{\text{u}} = \frac{Q(T_{\text{ex}})}{g_{\text{u}} \exp\left(-\frac{h\nu}{kT_{\text{ex}}}\right)}, \quad (12)$$

where g_{u} is the statistical weight of the upper level. T_{ex} is the excitation temperature and $Q(T_{\text{ex}}) = kT_{\text{ex}}/B_{\text{e}}$ is the LTE partition function, where B_{e} is the rotational constant (Tennyson 2005). The partition function can be expressed as $Q(T_{\text{ex}}) \approx T_{\text{ex}}/2.76$ K. The correction factor for opacity f_{τ} is defined as

$$f_{\tau} = \frac{\int \tau_{13} dv}{\int (1 - e^{-\tau_{13}}) dv}, \quad (13)$$

and the correction for the background f_{b} can be ex-

pressed as

$$f_{\text{b}} = \left[1 - \frac{e^{\frac{h\nu}{kT_{\text{ex}}}} - 1}{e^{\frac{h\nu}{kT_{\text{bg}}}} - 1} \right]^{-1}, \quad (14)$$

where τ_{13} is the opacity of the ^{13}CO transition and T_{bg} is the background temperature, which is assumed to be 2.7 K. The ^{13}CO opacity is estimated under the assumption of being optically thin, for which $f_{\tau} = 1$. The excitation temperature T_{ex} can be replaced by the dust temperature T_{d} . The maximum ^{13}CO column densities obtained using this analysis for the three sources B227, L1574, and CB45 are $4.1 \times 10^{15} \text{cm}^{-2}$, $4.9 \times 10^{15} \text{cm}^{-2}$, and $7.3 \times 10^{15} \text{cm}^{-2}$. We then derived the ^{13}CO abundance through column densities of dust and ^{13}CO with consideration of other chemical effects, like ^{13}CO depletion, and all of them are likely not dominant for our case.

Based on the dust data, the central volume densities of the three clouds, B227, L1574, and CB45 are 1600cm^{-3} , 2200cm^{-3} , and 1800cm^{-3} , assuming cloud sizes of 0.8 pc, 1.0 pc, and 1.5 pc respectively. The volume density is much greater than the ^{13}CO critical density of 1266cm^{-3} , confirming the validation of the LTE assumption.

3.4. Abundances

The abundances of HiNSA and ^{13}CO have been derived through a combined analysis with dust emission and extinction. We regarded the ratio between HI column density N_{HI} and H_2 column density N_{H_2} as HI abundance ($[\text{HI}]/[\text{H}_2]$). The ^{13}CO abundance is derived from the ratio between ^{13}CO column density $N_{^{13}\text{CO}}$ and H_2 column density N_{H_2} ($[^{13}\text{CO}]/[\text{H}_2]$). We identified a striking ‘‘ring’’ of enhanced HI abundance, which is the first time such a structure has been seen in a molecular cloud. It closely resembles the ‘‘onion’’ shell description of a forming molecular cloud (Figure 1). The displacement between peak abundance positions of HI, ^{13}CO , and dust indicates the ongoing H_2 formation. Particularly, we find an orderly spatial variation of HI abundance between 2% and 0.2%. The distribution of HI abundance measured from HiNSA is also consistent with the inner cloud ‘‘core’’ being chemically more evolved, due to higher volume densities present there.

4. MODEL

4.1. H_2 Formation Model

H_2 formation occurs on the dust grain with a formation rate (Hollenbach & Salpeter 1971)

$$R_{\text{H}_2} = \frac{1}{2} S_{\text{HI}} \epsilon_{\text{H}_2} n_{\text{HI}} \langle v_{\text{HI}} \rangle \sigma_{\text{gr}} n_{\text{gr}}, \quad (15)$$

where R_{H_2} has units of $\text{cm}^{-3} \text{s}^{-1}$, S_{HI} is the sticking efficiency, ϵ_{H_2} is the recombination efficiency, n_{gr} (cm^{-3}) is the atomic hydrogen density in the gas, $\langle v_{\text{HI}} \rangle$ (cm s^{-1}) is the mean velocity of atoms, σ_{gr} (cm^2) is the cross section of grains, and n_{gr} (cm^{-3}) is the number density of grains.

The values and derivations of the parameters are taken from Goldsmith & Li (2005). The simplification of the

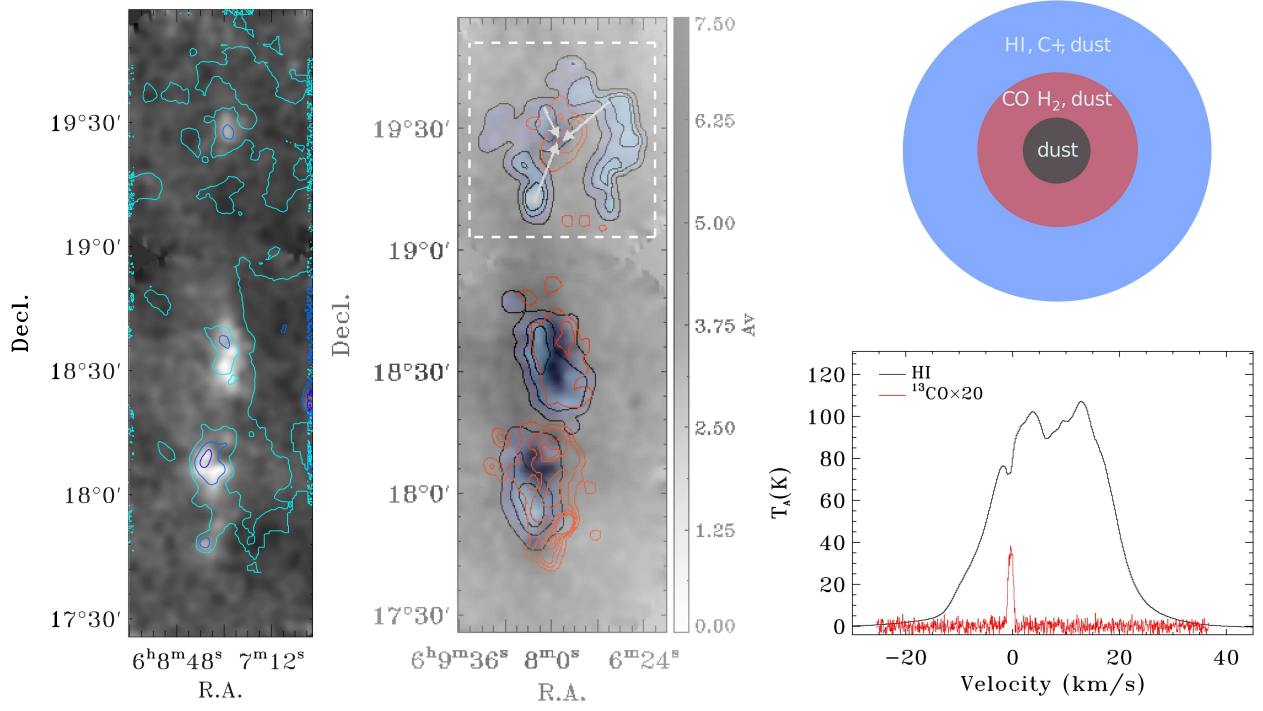


Figure 1. Temperature distribution, abundance distribution, onion-like model, and HiNSA feature. Left: the 2MASS extinction overlaid with the dust temperature. The contours from light blue to dark blue are 12 K, 13 K, and 14 K respectively. Middle: the 2MASS extinction overlaid with the ratio of $[\text{HI}]/[\text{H}_2]$ column densities (black contour and blue shadow), and $[\text{^{13}CO}]/[\text{H}_2]$ column density (red) respectively. The black contours are at 10%, 40%, and 70% of maximum value of 2.1×10^{-2} . The red contours are at 10%, 30%, 50%, 70%, and 90% of maximum value. The maximum value is 2.1×10^{-6} . The white arrows show the direction of the HI-H₂ transition of B227. Right top: an onion-like model of evolving molecular cloud, which is a 2D version of the left image, corresponding to the source B227. Right bottom: HiNSA feature of the source B227 at velocity $\simeq -1 \text{ km s}^{-1}$, with corresponding ^{13}CO emission, which is from the center of B227.

H₂ formation rate can be expressed as

$$R_{\text{H}_2} = k_{\text{H}_2} n_{\text{gas}} n_{\text{HI}}. \quad (16)$$

We denote the H₂ formation rate coefficient k_{H_2} as $k' = 1.2 \cdot 10^{-17} \text{ cm}^3 \text{ s}^{-1}$ after taking the effect of grain size distribution into account (Goldsmith & Li 2005).

The formation rate coefficient k' is related to the grain size, namely the cross-section area of dust grains, which is connected to the thermal balance and the estimate of dust mass. Based on the study of grain size distribution from Mathis et al. (1977), the reasonable upper and lower limits of radii, $a_{\text{max}} = 10000 \text{ \AA}$ and $a_{\text{min}} = 25 \text{ \AA}$, which enter as $(a_{\text{max}} a_{\text{min}})^{-0.5}$, are adopted for evaluating the effect of the grain size distribution on the formation rate coefficient. In comparison with the standard grain radius 1700 \AA , the formation rate coefficient is increased by a factor of 3.4. Combining the grain size distribution and other factors, the uncertainty of H₂ formation rate coefficient may differ from its nominal value by a factor of 5. Although the nominal value of k' we take has large uncertainty, it is well beyond the goal of this paper to consider the overall context. Therefore, we are utilizing the most common value for the cross-section area of the dust.

The density of gas n_{gas} can be regarded as total density n_0 as $n_0 \propto n_{\text{gas}}$. We derived the volume proton density of the clouds through the dust data. For the volume proton density, we derived the mean values from outer to inner

of the cloud by assuming the cloud is spherical. It ranges from $10^{2.9} \text{ cm}^{-3}$ to $10^{3.2} \text{ cm}^{-3}$ approximately (Figure 2). The time dependence of the molecular hydrogen can be express as

$$\frac{dn_{\text{H}_2}}{dt} = k' n_{\text{HI}} n_0 - \zeta_{\text{H}_2} n_{\text{H}_2}, \quad (17)$$

where ζ_{H_2} is the cosmic-ray ionization rate. We defined the fractional abundance of atomic and molecular hydrogen, x_{HI} and x_{H_2} , as the density of species n_{HI} and n_{H_2} divided by the total proton density n_0 , then we find

$$\frac{dx_{\text{H}_2}}{dt} = k' x_{\text{HI}} n_0 - \zeta_{\text{H}_2} x_{\text{H}_2}. \quad (18)$$

Substituting $n_0 = n_{\text{HI}} + n_{\text{H}_2}$, we can rewrite this as

$$\frac{dx_{\text{H}_2}}{dt} = k' n_0 - (2k' n_0 + \zeta_{\text{H}_2}) x_{\text{H}_2}. \quad (19)$$

The time dependence of the fractional abundance of molecular hydrogen is then given by

$$x_{\text{H}_2}(t) = \frac{k' n_0}{2k' n_0 + \zeta_{\text{H}_2}} [1 - \exp(\frac{-t}{\tau_{\text{HI} \rightarrow \text{H}_2})}]. \quad (20)$$

The fractional abundance of atomic hydrogen is $1 - 2x_{\text{H}_2}$ and is given by

$$x_{\text{HI}}(t) = 1 - \frac{2k' n_0}{2k' n_0 + \zeta_{\text{H}_2}} [1 - \exp(\frac{-t}{\tau_{\text{HI} \rightarrow \text{H}_2})}]. \quad (21)$$

The timescale for HI to H₂ conversion is given by

$$\tau_{\text{HI} \rightarrow \text{H}_2} = \frac{1}{2k'n_0 + \zeta_{\text{H}_2}}. \quad (22)$$

We derived the timescales of these isolated dark clouds to be ~ 6 Myrs using HI abundance, total gas density, and gas temperature obtained according to the time dependence model described in this section (Figure 2). The upper and lower limits of HI abundances are plotted in Figure 2 and the points at upper limits represent the lower ages of the clouds for the fixed volume densities.

4.2. Chemical Model

We also use a two-stage young dark clouds formation collapse model. We assume that translucent clouds are the intermediate stage when diffuse clouds become young dark clouds. In the first stage, when diffuse clouds become translucent clouds, we only consider the HI \rightarrow H₂ transition process as discussed in the rest of the paper. In the second stage, we simulate a gas–grain reaction network to calculate the chemical evolution of species including HI and H₂ in collapsing cores.

We use the Ohio State University (OSU) gas–grain code. The gas–grain chemical reaction network is explained in [Hincelin et al. \(2011\)](#) and [Hincelin et al. \(2013\)](#). Moreover, the Kinetic Database for Astrochemistry (KIDA) database ([Wakelam et al. 2012](#)) also has an electronic version of the network. We simulate the gas–grain chemistry in free-fall collapsing cores with initial hydrogen nucleus densities of $10^{2.3}$ and $10^{2.4}$ cm⁻³ and evolve to $10^{3.2}$ and $10^{3.3}$ cm⁻³ eventually. It takes 10^7 years to collapse to form a dense core. During free-fall collapse, the rate at which the density increase is given by [Spitzer \(1978\)](#). The collapsing process is isothermal with a constant temperature of 10 K while the visual extinction varies from 1 to 4 mag. The cosmic-ray ionization rate is set to 5.2×10^{-17} s⁻¹. The size of dust grains is assumed to be uniform, with a radius of 0.1 μ m. The sticking coefficient is fixed to be 1. The elemental abundances are assumed to be “low metal,” as in [Semenov et al. \(2010\)](#). In our model, species in the young dark clouds are formed by the chemical evolution of species in translucent clouds. Thus, we use the observed abundances of species in translucent clouds in HD 24534, HD 154368 and HD 210121 ([Sofia et al. 2004](#); [Sonnentrucker et al. 2007](#); [Weselak et al. 2009](#); [Burgh et al. 2010](#)) where the atomic H density is about a quarter of the total H nucleus density of the initial abundances in our calculation of the second stage. If a species is observed in more than one source, we take the average of the observed values in different sources. Table 1 shows the initial abundances used in our calculation. Through this time-dependent chemical model, we compared the timescales of cloud evolution traced by the abundance of HI and CO with our observed abundances and calculated timescale. The observed HI abundance and timescale of cloud formation is partially consistent with the chemical model. On the other hand, CO abundance is only marginally consistent with the chemical model, which already evolved into the steady state at the corresponding abundance (Figure 2).

5. DISCUSSION

Table 1
Initial abundances used in the chemical model

Element	Abundance
C	4.34×10^{-7}
H	2.50×10^{-1}
He	9.00×10^{-2}
N	7.60×10^{-5}
O	2.50×10^{-4}
C ₂	1.79×10^{-8}
CH	1.59×10^{-8}
CN	6.79×10^{-9}
CO	5.45×10^{-6}
H ₂	3.75×10^{-1}
NH	1.78×10^{-9}
OH	4.36×10^{-8}
C ⁺	1.14×10^{-4}
Cl ⁺	1.00×10^{-9}
Fe ⁺	3.00×10^{-9}
Mg ⁺	7.00×10^{-9}
Na ⁺	2.00×10^{-9}
P ⁺	2.00×10^{-10}
S ⁺	8.00×10^{-8}
Si ⁺	8.00×10^{-9}
CH ⁺	5.51×10^{-9}
e	1.14×10^{-4}

It has been rare to have both HI and H₂ measured for the same regions in the Galaxy. [Lee et al. \(2015\)](#) used the integrated HI emission flux in channels, the range of which was determined by correlation with 2MASS extinction. Such a priori requirements of HI mimicking dust diminish the logical credence of HI emission being tracing the atomic component within a molecular cloud. [Fukui et al. \(2014\)](#) found an optically thick HI emission envelope around a molecular cloud. In this work, utilizing HiNSA, we discovered a chemically young molecular cloud undergoing H₂ formation, revealed by a prominent “ring” of self-absorption tracing atomic hydrogen mixed with molecules. We derived the formation timescale to be ~ 6 Myr, consistent with both an analytical model and a numerical chemistry model. Our results could further test recent H₂ formation models in different contexts ([Sternberg et al. 2014](#); [Bialy et al. 2017](#)).

Our results can also help constrain galaxy evolution simulations. A key recent development is the implementation of the physics of molecular hydrogen and star formation prescription based on the local molecular hydrogen density rather than the total hydrogen density ([Zemp et al. 2012](#)). In [Gnedin & Kravtsov \(2011\)](#), only two types of observations were able to calibrate the H₂ formation rate in different environments, UV absorption in diffuse regions and HiNSA in dense clouds. This work further improves the accuracy of the HiNSA measured H₂ formation rate.

Both the timescale and HI abundance distribution of the clouds are inconsistent with fast H₂ formation ([Glover & Mac Low 2007](#)), which relies on stochastic processes of localized high volume HI density. Such a fast cloud formation model could produce a significant amount of molecular hydrogen, e.g. for cooling in a short time, but cannot convert the vast majority of the gas into molecular form, which is our key finding here. The fact that more than 99% of the protons have

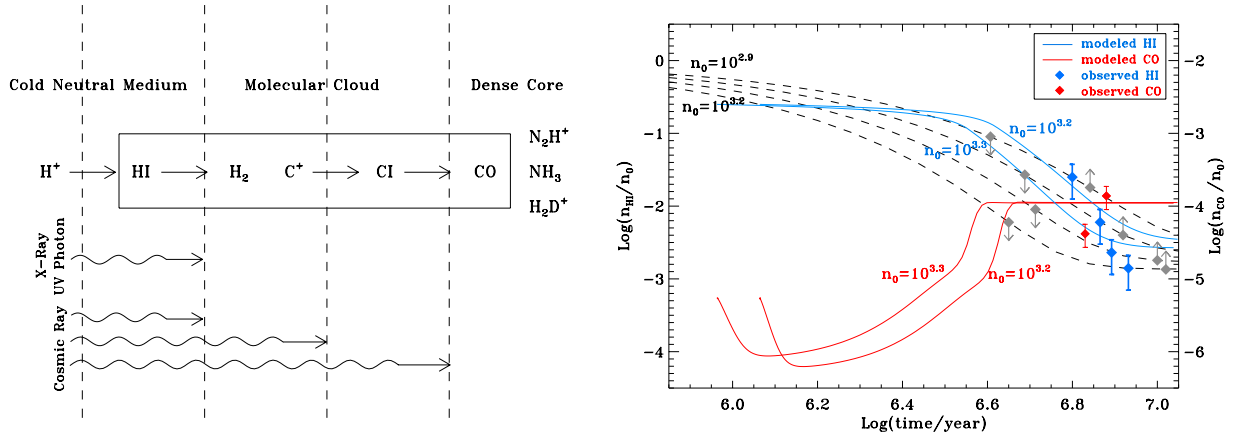


Figure 2. Chemical process and time-dependent model. Left: the chemical processes of diffuse CNM–molecular cloud–dense core. The processes in the square indicates the chemical evolution in our work, which is corresponding to the right plot. Right: time dependence of the fractional abundance of the atomic hydrogen and CO. The blue and red symbols represent the HI and CO observations, respectively. The four HI measurements are from the four points that are along the right top arrow of source B227 in Figure 1. The two CO measurements (from left to right) are the mean values from the outer envelop and inner core of the source B227, and the mean proton total densities are $10^{2.9} \text{ cm}^{-3}$ and $10^{3.0} \text{ cm}^{-3}$ respectively. The dashed lines represent the H_2 formation model for clouds at different total proton densities n_0 . The blue and red lines represent the cloud evolution in a time-dependent model with the abundance of HI and CO. The gray diamonds with upward and downward arrows represent the lower and upper limits of the HI abundances.

been turned into H_2 requires millions of the years and comprehensive global H_2 formation, not just in pockets of locally enhanced condensations. The observed Mach number of the clouds is more than 20, which elevates the inconsistency between our observation and the fast cloud formation model.

The total column densities found in these isolated dark clouds are consistent with commonly used initial conditions for protoplanetary disks. However, the measured HI abundance is one to a few orders of magnitude higher than those assumed in such models (e.g. Walsh et al. 2015). In these models, the HI abundance keeps dropping with time and impacts subsequent chemical reactions. We expect our measured value to affect future consideration of chemical evolution of disks. All the above statements indicate that the parameters of galactic H_2 formation play a crucial role in both galaxy evolution and star formation.

6. SUMMARY

We mapped HI, $^{13}\text{CO } J = 1 - 0$ emission, and dust continuum emission of isolated dark clouds, B227, CB45, and L1574. The combined analysis of HiNSA, CO emission, dust emission, and extinction enables us to directly measure the variation HI abundance in these transition clouds. The timescale of the clouds had been examined through an analytical model. Our main results are the following.

- : 1. We identified a striking “ring” of enhanced HI abundance, which is the first time such a structure has been seen in a molecular cloud. It closely resembles the “onion” shell description of a forming molecular cloud (Figure 1). The displacement between peak abundance positions of HI, CO, and dust indicates the ongoing H_2 formation. Particularly, we find an orderly spatial variation of HI abundance between 2% and 0.2%.

- : 2. We derived the HI– H_2 evolutionary timescales for these isolated dark clouds to be ~ 6 Myr and further examined the cloud evolution through a time-dependent chemical model.
- : 3. Our results could test H_2 formation models, constrain galaxy evolution simulations, and may affect future consideration of chemical evolution of disks, all of which indicate that the parameters of galactic H_2 formation play a crucial role for both galaxy evolution and star formation.

This work is supported by National Key R&D Program of China grant No. 2017YFA0402600, the National Natural Science Foundation of China grant No. 11725313 and No. 11690024, and the International Partnership Program of Chinese Academy of Sciences grant No. 114A11KYSB20160008. The Arecibo Observatory is operated by SRI International under a cooperative agreement with the National Science Foundation (AST-1100968), and in alliance with Ana G. Méndez-Universidad Metropolitana, and the Universities Space Research Association. D.L. acknowledges support from “CAS Interdisciplinary Innovation Team” program. This work was carried out in part by the Jet Propulsion Laboratory, which is operated by NASA through the California Institute of Technology. Z.Y.Z. acknowledges support from ERC in the form of the Advanced Investigator Programme, 321302, COSMICISM.

REFERENCES

- Bergin, E. A., Hartmann, L. W., Raymond, J. C., & Ballesteros-Paredes, J. 2004, *ApJ*, 612, 921
- Bialy, S., Bihl, S., Beuther, H., Henning, T., & Sternberg, A. 2017, *ApJ*, 835, 126
- Brünken, S., Sipilä, O., Chambers, E. T., et al. 2014, *Nature*, 516, 219
- Burgh, E. B., France, K., & Jenkins, E. B. 2010, *ApJ*, 708, 334
- Caselli, P., Benson, P. J., Myers, P. C., & Tafalla, M. 2002, *ApJ*, 572, 238
- Cazaux, S., Caselli, P., Tielens, A. G. G. M., LeBourlot, J., & Walmsley, M. 2005, *Journal of Physics Conference Series*, 6, 155
- Cazaux, S., & Tielens, A. G. G. M. 2004, *ApJ*, 604, 222
- Elmegreen, B. G. 2000, *ApJ*, 530, 277
- Fukui, Y., Okamoto, R., Kaji, R., et al. 2014, *ApJ*, 796, 59
- Gibson, S. J., Taylor, A. R., Higgs, L. A., & Dewdney, P. E. 2000, *ApJ*, 540, 851
- Glover, S. C. O., & Mac Low, M.-M. 2007, *ApJ*, 659, 1317
- Gnedin, N. Y., & Kravtsov, A. V. 2011, *ApJ*, 728, 88
- Goldsmith, P. F., & Li, D. 2005, *ApJ*, 622, 938
- Güver, T., & Özel, F. 2009, *MNRAS*, 400, 2050
- Heeschen, D. S. 1955, *ApJ*, 121, 569
- Heiles, C., & Troland, T. H. 2003, *ApJ*, 586, 1067
- Hincelin, U., Wakelam, V., Commerçon, B., Hersant, F., & Guilloteau, S. 2013, *ApJ*, 775, 44
- Hincelin, U., Wakelam, V., Hersant, F., et al. 2011, *A&A*, 530, A61
- Hollenbach, D., & Salpeter, E. E. 1971, *ApJ*, 163, 155
- Kaiser, R. I. 2002, *Chemical Reviews*, 102, 155
- Knee, L. B. G., & Brunt, C. M. 2001, *Nature*, 412, 308
- Kolpak, M. A., Jackson, J. M., Bania, T. M., & Dickey, J. M. 2002, *ApJ*, 578, 868
- Kramer, C., Alves, J., Lada, C. J., et al. 1999, *A&A*, 342, 257
- Krčo, M., & Goldsmith, P. F. 2010, *ApJ*, 724, 1402
- Lee, M.-Y., Stanimirović, S., Murray, C. E., Heiles, C., & Miller, J. 2015, *ApJ*, 809, 56
- Li, D., & Goldsmith, P. F. 2003, *ApJ*, 585, 823
- Martin, R. N., & Barrett, A. H. 1978, *ApJS*, 36, 1
- Mathis, J. S., Rumpl, W., & Nordsieck, K. H. 1977, *ApJ*, 217, 425
- Minchin, R. F., Auld, R., Davies, J. I., et al. 2007, *Galaxy Evolution across the Hubble Time*, 235, 227
- Peek, J. E. G., Heiles, C., Douglas, K. A., et al. 2011a, *ApJS*, 194, 20
- Peek, J. E. G., Heiles, C., Peek, K. M. G., Meyer, D. M., & Lauroesch, J. T. 2011b, *ApJ*, 735, 129
- Sembach, K. R., Howk, J. C., Savage, B. D., & Shull, J. M. 2001, *AJ*, 121, 992
- Semenov, D., Hersant, F., Wakelam, V., et al. 2010, *A&A*, 522, A42
- Shu, F. H. 1977, *ApJ*, 214, 488
- Sofia, U. J., Lauroesch, J. T., Meyer, D. M., & Cartledge, S. I. B. 2004, *ApJ*, 605, 272
- Sonnentrucker, P., Welty, D. E., Thorburn, J. A., & York, D. G. 2007, *ApJS*, 168, 58
- Spitzer, L., Jr. 1946, *Publications of the American Astronomical Society*, 10, 144
- Spitzer, L. 1978, *Physical processes in the interstellar medium*, by Lyman Spitzer. New York Wiley-Interscience, 1978. 333 p., Sternberg, A., Le Petit, F., Roueff, E., & Le Bourlot, J. 2014, *ApJ*, 790, 10
- Tennyson, J. 2005, *Astronomical spectroscopy : an introduction to the atomic and molecular physics of astronomical spectra*, by J. Tennyson. Imperial College Press advanced physics texts, vol. 2 London: Imperial College Press, 2005 ISBN 9781860946790,
- Vidali, G., Roser, J., Manicó, G., et al. 2005, *Journal of Physics Conference Series*, 6, 36
- Wakelam, V., Herbst, E., Loison, J.-C., et al. 2012, *ApJS*, 199, 21
- Walsh, C., Nomura, H., & van Dishoeck, E. 2015, *A&A*, 582, A88
- Weselak, T., Galazutdinov, G. A., Beletsky, Y., & Krelowski, J. 2009, *MNRAS*, 400, 392
- Woodall, J., Agúndez, M., Markwick-Kemper, A. J., & Millar, T. J. 2007, *A&A*, 466, 1197
- Zemp, M., Gnedin, O. Y., Gnedin, N. Y., & Kravtsov, A. V. 2012, *ApJ*, 748, 54